Received 27 January 2023; revised 21 February 2023; accepted 28 February 2023. Date of publication 6 March 2023; date of current version 17 March 2023.

Digital Object Identifier 10.1109/OJAP.2023.3252676

Ultra-Wideband 3-D Microwave Absorbers With Composite Slotlines and Microstrip Lines: Synthetic Design and Implementation

TIAN-XI FENG (Graduate Student Member, IEEE), AND LEI ZHU (Fellow, IEEE)

Department of Electrical and Computer Engineering, Faculty of Science and Technology, University of Macau, Macau, China

CORRESPONDING AUTHOR: L. ZHU (e-mail: leizhu@um.edu.mo)

This work was supported in part by the National Natural Science Foundation of China through the General Program under Grant 61971475, and in part by the Macao Science and Technology Development Fund through FDCT Research Grants under Grant 0085/2020/AMJ and Grant 0080/2021/A2.

ABSTRACT This article proposes a class of ultra-wideband 3-D microwave absorbers with composite slotlines and microstrip lines from synthetic design to practical implementation. Firstly, the general equivalent transmission line (TL) model of the proposed 3-D absorber element is formed based on two sets of shunt short-ended stubs and an i-section nonuniform connecting line. Then, the synthetic procedure is theoretically investigated using the equivalent TL model, aiming to construct an ultra-wide absorption band with the Chebyshev equal-ripple response. According to the prescribed absorptive performance, such as maximum reflection coefficient (Γ) and fractional bandwidth (FBW), the relevant parameters of the TL model can be directly calculated by the established synthesis approach. To validate the proposed concept, two prototypes, namely, absorber-I ($i = 1$) and absorber-II ($i = 2$), are designed, fabricated, and measured. Each prototype element applies a simple 3-D structure composed of slotlines, microstrip lines, and only one absorptive load, which are all etched on a single-layered substrate. Measured results agree well with synthetizations and simulations. For absorber-I, the measured bandwidth of 95.5% in a frequency range from 5.08 to 14.44GHz is successfully realized. Absorber-II obtains a measured FBW of 111.1% in a range from 4.48 to 15.68GHz. Average absorption ratios within the operating band are higher than 95.5% and 93.8% for absorber-I and absorber-II, respectively. Besides, the proposed 3-D absorbers are angularly stable within 60° oblique incidence. Therefore, such ultra-wideband 3-D microwave absorbers with simple structures possess the attractive potential for effectively absorbing electromagnetic waves.

INDEX TERMS 3-D microwave absorber, equivalent transmission line model, synthetic design, ultra-wideband absorber.

I. INTRODUCTION

MICROWAVE absorbers have been widely used in varieties of applications for electromagnetic (EM) manipulations, such as antenna design, radar camouflage, electromagnetic compatibility (EMC), or measurement system [1]. With the rapid development of modern wireless systems, wider absorption bands are highly demanded in absorber designs for the complicated EM environment.

Conventional two-dimensional (2-D) absorbers, such as Dallenbache layer and Salisbury screen, were obtained based on a lossy dielectric or resistive screen [2], [3]. In order to realize a wider absorptive band, multilayer resistive screens were employed in the Jaumann absorber [4]. For further improvement of the operating bandwidth, different materials were introduced into absorber designs [5], [6], [7], [8], [9], [10], [11], [12]. The ferrite backed with a conducting plate in [5] is applied to design a perfect absorber at the operating frequency. In [6], wideband absorbers with a single-layer substrate were explored utilizing periodic square resistive patches. To design a bandwidth- tunable absorber, graphene sheets were used in [7] to dynamically tune the surface impedance. In [8], the frequency- dispersive magnetic material was employed to obtain an ultrathin absorber with increased bandwidth. To design a wideband

polarization-insensitive multilayered absorber, the resistive ink was utilized in [9] for periodic resistive patterns. In [10], the ultra-wideband water-based microwave absorber was reported with angle and temperature stability. Using sustainable waste biomass, a simple and economical structural absorber was presented in [11] with enhanced absorption performance. In [12], an all-dielectric ultra-wideband absorber was realized using a resin shell and saline structure.

Another popular approach to designing wideband absorbers is loading lumped resistors in a circuit analog way [13], [14], [15], [16], [17]. In [13], a wideband single-layer absorber was designed by utilizing double-square-loop array loading with lumped resistors. Using slot arrays loaded with resistors, a switchable low-profile wideband rasorber/absorber was presented in [14]. In [15], chip-resistors were embedded into metallic strips to realize a wideband absorber under multimode operation. For the design of an active absorber with ultrawide bandwidth and extremely low profile, non-foster devices and resistors were employed in [16]. In [17], an active tunable absorber was presented to obtain the ultrawide bandwidth.

Apart from the 2-D microwave absorbers mentioned above, the class of 3-D absorbers, which is based on the 2-D periodic structure of transmission lines, has been attracting considerable interest recently [18], [19], [20], [21], [22], [23], [24], [25], [26], [27], [28], [29], [30], [31], [32]. Based on a 2-D array of microstrip lines, the authors in [18] proposed the modeling and design of a wideband circuit analog absorber. In [19] and [20], the concept of 3-D frequency selective rasorbers was presented with wide absorption bandwidths. Based on resistor-loaded strip lines, different 3-D absorptive structures were realized in [21], [22], [23], [24] for wideband performance. In [25] and [26], the honeycomb structure was employed to obtain wide bandwidths with reduced weight. To realize a 3-D frequency-selective rasorber with wide absorption bandwidth, the multilayer structure and magnetic ferrite were utilized in [27]. Combining the ferrite and a slow wave structure, the rasorber in [28] realized the wide absorption band and the ultrathin profile. In [29], the bistatic radar cross section reduction was obtained via introducing the spoof surface plasmon polariton (SSPP) structure into the absorber design. By controlling multiple resistive electric and magnetic resonances, a low-profile wideband microwave absorber was presented in [30]. In [31], the via-based hybrid metal-graphene metamaterial was employed to realize a wideband absorber with miniaturized periodicity. Using the cascaded multi-layered planar magnetic absorber, the absorptive transmission structure in [32] realized an extended absorption band.

In this article, we try to propose the synthetic design and implementation of a class of ultra-wideband 3-D microwave absorbers with composite slotlines and microstrip lines. Firstly, we construct the general equivalent transmission line (TL) model of the proposed 3-D absorber element based on two sets of shunt short-ended stubs and an i-section nonuniform connecting line. The equivalent model is then utilized for the theoretical synthetic procedure, which aims to establish an ultrawide absorption band with the Chebyshev equal-ripple response. Using the above synthesis approach, the relevant parameters of the TL model can be directly calculated according to the specifications of absorptive performance, such as maximum reflection coefficient (Γ) and fractional bandwidth (FBW). To prove our presented concept, two prototypes, namely, absorber-I ($i = 1$) and absorber-II ($i = 2$), are designed, fabricated, and measured. For each prototype element, a single-layered substrate is employed to obtain the very simple 3-D structure, which consists of slotlines, microstrip lines, and only one absorptive load. Measured results agree well with synthetizations and simulations. As for absorber-I, the measured (simulated) bandwidth of 95.5% in a frequency range from 5.08 to 14.44GHz (94.9% from 5.18 to 14.54GHz) is successfully realized. Absorber-II realizes a measured (simulated) bandwidth of 111.1% in a range from 4.48 to 15.68GHz (112.2% from 4.37 to 15.54GHz). Within the operating band, measured average absorption ratios (ARs) for absorber-I and absorber-II are higher than 95.5% and 93.8%, respectively. In addition, the proposed 3-D absorbers possess angular stability within 60° oblique incidence. Therefore, such ultra-wideband 3-D microwave absorbers with simple structures own their potential for EM waves absorption.

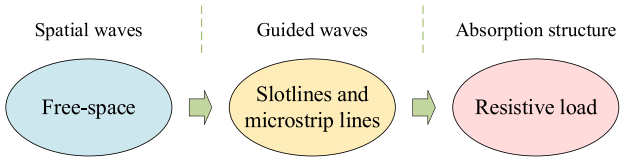

FIGURE 1. Working strategy of the proposed 3-D absorber.

The remainder of this article is organized as follows. In Section II, the operation principle of the proposed 3-D absorber element is investigated, including the working strategy, the equivalent TL model, and the synthetic procedure. Section III detailly describes the implementation and measurement of two prototypes for validating the proposed concept. Finally, the conclusion is briefly presented in Section IV.

II. OPERATION PRINCIPLE

Fig. 1 conceptually describes the working strategy of the proposed 3-D absorber. The incoming spatial waves from free-space impinge on the proposed 3-D absorber and then are effectively converted into the guided waves at the interface. After that, the guided waves propagate along the transmission lines, such as slotlines and microstrip lines. Finally, the guided waves are fully absorbed by a resistive load. Under this condition, the keys to obtain the proposed ultra-wideband absorber are establishing a symmetric equivalent model and realizing a 3-D structure.

Fig. 2 depicts the equivalent TL model of the proposed 3-D absorber element, which is mainly composed of two

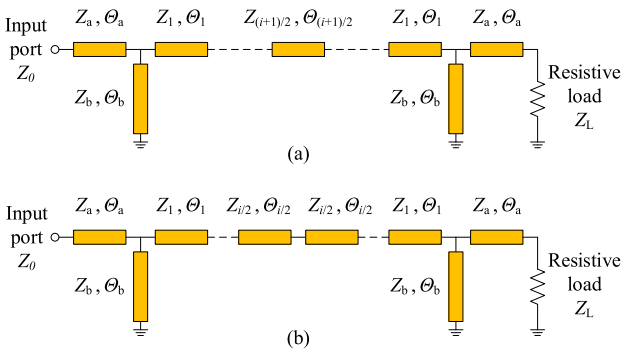

FIGURE 2. Equivalent transmission line model of the proposed 3-D absorber element based on shunt short-ended stubs and an *i*-section nonuniform connecting line. (a) *i* is odd-integer (1, 3, 5, . . .). (b) *i* is even-integer (0, 2, 4, . . .).

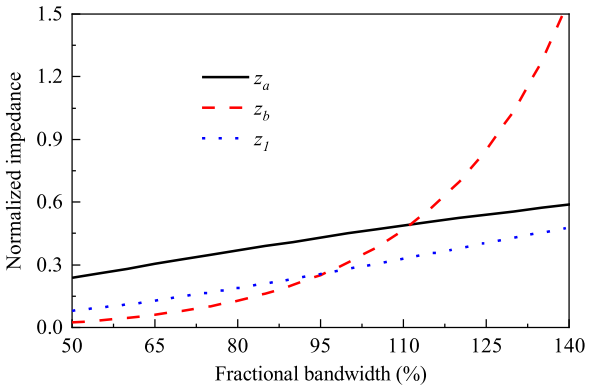

FIGURE 3. Normalized characteristic impedances of z_a, z_b, and z_1 for different fractional bandwidths under $\Gamma = -10$dB when $i = 1$.

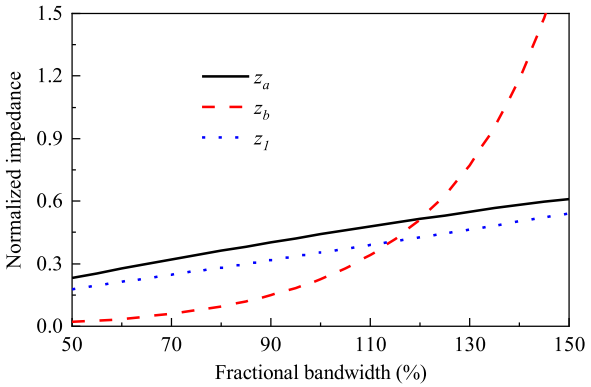

FIGURE 4. Normalized characteristic impedances of z_a, z_b, and z_1 for different fractional bandwidths under $\Gamma = -10$dB when $i = 2$.

sets of shunt short-ended stubs and an i-section nonuniform connecting line. It is shown in Fig. 2(a) and Fig. 2(b) for the odd- and even-integer i, respectively. The characteristic impedances and electrical lengths of each TL are Z_m and Θ_m (m = a, b, 1, 2, 3, . . .). In this work, all TLs are set with the same electrical length of $\lambda/4$ at the center frequency in the desired operating band. Besides, the input spatial wave impedance Z_0 is equal to the terminal absorptive load Z_L, which results in the equivalent TL model being horizontally symmetrical. It is worth noting that the output port is replaced by an absorptive resistor, thus the characteristic function of the equivalent model can be used to evaluate the absorptive performances.

For the universality, two examples ($i = 1$ and $i = 2$) are illustrated using the synthetic procedure similar to [33], [34]. As for to $i = 1$, the characteristic function of the equivalent TL model is derived as

$$F^I = j\left(k_1 \frac{\cos^4\theta}{\sin\theta} + k_2 \frac{\cos^2\theta}{\sin\theta} + k_3 \frac{1}{\sin\theta}\right) \tag{1}$$

The coefficients of k_1, k_2, and k_3 are given by (A-1) in the Appendix. In this work, all the characteristic impedances are normalized with respect to Z_0, that is $z_m = Z_m/Z_0$ (m = a, b, 1, 2, 3, . . .).

When $i = 2$, the characteristic function can be calculated using the same synthesis approach as

$$F^{II} = j\left(l_1 \frac{\cos^5\theta}{\sin\theta} + l_2 \frac{\cos^3\theta}{\sin\theta} + l_3 \frac{\cos\theta}{\sin\theta}\right) \tag{2}$$

The coefficients of l_1, l_2, and l_3 are given by (A-2) in the Appendix. By equalizing the coefficients k_1–k_3, l_1–l_3, and the corresponding coefficients of the Chebyshev function, the normalized characteristic impedances can be explicitly determined by the specified absorptive performance.

To provide more design selection for ultra-wideband absorbers, Fig. 3 shows normalized characteristic impedances of z_a, z_b, and z_1 with respect to different fractional bandwidths under $\Gamma = -10$dB when $i = 1$. The normalized characteristic impedances under $i = 2$ for $\Gamma = -10$dB are shown in Fig. 4. All impedances demonstrate similar increasing trends with the rise of the fractional bandwidth. From these theoretical results, it is clear that the proposed equivalent TL model can be employed to directly design ultra-wideband microwave absorbers using the above synthesis approach.

III. IMPLEMENTATION AND VERIFICATION

To verify the proposed concept, two prototype examples of absorber-I and absorber-II are illustrated in this section from element design to array implementation.

A. ABSORBER-I

Fig. 5 shows the element configuration of the proposed 3-D absorber-I ($i = 1$), where slotlines, microstrip lines, and one absorptive load are etched on a single-layered substrate. In this work, the resistive film from Ohmega (377Ohm/square) is employed to form the absorptive load. The FR4 substrate with a relative permittivity of 4.4 and a dielectric loss tangent of 0.0166 is used for our design. To better clarify the relationship between the structural design and the equivalent model, each section of transmission lines is highlighted with corresponding marks. As seen in Fig. 5(b), two sections of the slotline are designed on the backside ground, resulting in the conversion from y-polarized spatial waves in free space to guided waves in the slotline. The first section of slotline

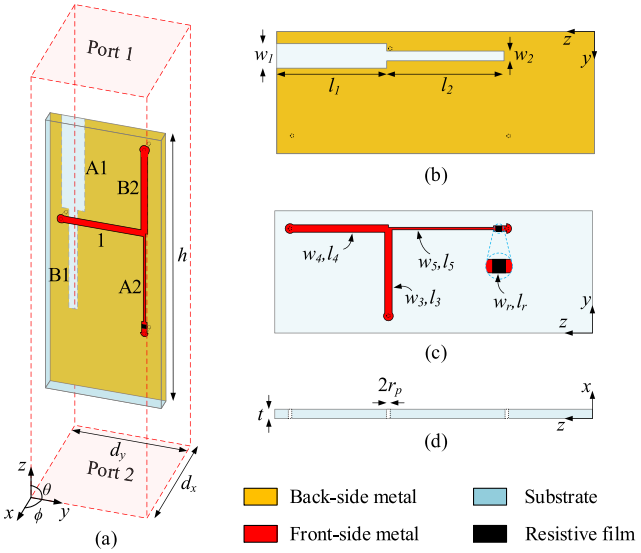

FIGURE 5. Element geometry of the proposed 3-D absorber-I. (a) Perspective view. (b) Back view. (c) Front view. (d) Side view.

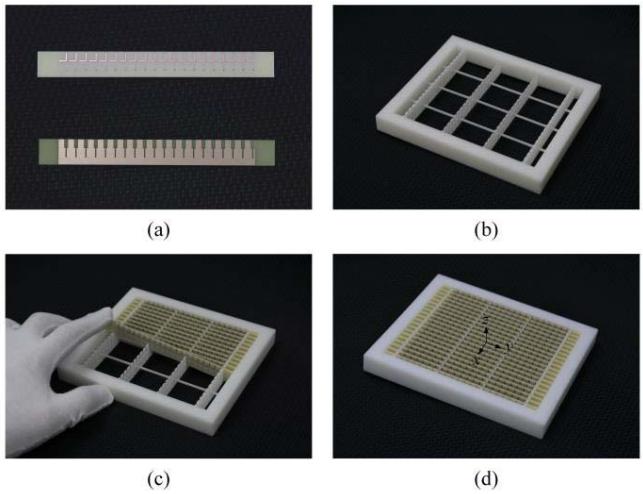

FIGURE 6. Photographs of the proposed 3-D absorber-I. (a) Substrate pieces. (b) 3-D printed fixing structure. (c) Fabrication procedure. (d) Final prototype.

TABLE 1. Geometrical parameters of the proposed 3-D absorber-I.

Parameter	d_x	d_y	h	t	w_1	l_1
Value (mm)	5	5	13	1.5	2	4.5
Parameter	w_2	l_2	w_3	l_3	w_4	l_4
Value (mm)	0.6	4.8	0.47	3.58	0.47	4.03
Parameter	w_5	l_5	w_r	l_r	r_p	
Value (mm)	0.1	4.3	0.22	0.22	0.1	

A1 (w_1, l_1) represents the first TL (Z_a, Θ_a) in the equivalent model. The short-circuited slotline B1 (w_2, l_2) denotes the first shunt short-ended stubs (Z_b, Θ_b). In Fig. 5(c), three sections of the microstrip line are etched on the front side and grounded through three shorting pins. Among them, the first section of microstrip line 1 (w_3, l_3) not only acts as the connecting line (Z_1, Θ_1), but also transits the guided wave from slotlines to microstrip lines. The microstrip line B2 with a size of (w_4, l_4) is the second shunt short-ended stub (Z_b, Θ_b). The third section of microstrip line A2 (w_5, l_5) represents the last TL (Z_a, Θ_a) in the equivalent model. In this geometry, only the y-polarized wave is supportable owing to the 3-D structure with one piece of the substrate. To overcome this polarization sensitivity, the proposed single-polarized design can be extended to a dual-polarized version by simply employing the cross-inserted structure.

Using the synthesis approach in Section II, the normalized characteristic impedances can be calculated as $z_a = 0.45$, $z_b = 0.31$, and $z_1 = 0.28$ with the prescribed absorptive performances of $\Gamma = -10$dB, FBW $= 100\%$. For absorber-I, the input impedance is set as $Z_0 = 377$Ohm, which is related to the element distance along the x and y directions. The width and length of each slotline can be obtained by simulating an individual slotline in a periodic element for the desired characteristic impedance and electrical length. The sizes of microstrip lines are easily attained from the microstrip line calculator. To minimize unwanted discontinuities, the size of the resistive film is designed to be as small as possible under the limitation of manufacturing accuracy. The optimized geometrical parameters are determined based on the above results and then shown in Table 1.

Fig. 6 describes photographs of the proposed 3-D absorber-I with detailed fabrication stages. It can be observed in Fig. 6(a) that each set of 20 elements is printed on a long piece of substrate. In addition, the substrate is extended by 10mm at two edges without etching metal to provide the convenience of fixation. The total size of the substrate for absorber-I is 120mm $\times$ 13mm. As shown in Fig. 6(b), a 3-D printed fixing structure is designed with the photosensitive resin material to realize structural stability and accuracy. Fig. 6(c) shows the fabrication procedure, where each substrate is inserted into securing slots for the proper spacing of the element. After that, the fabricated prototype with 20 $\times$ 20 elements is shown in Fig. 6(d).

To test the reflection coefficient and transmission coefficient of the prototype, the measurement system is set up as shown in Fig. 7. The transmitting antenna (Tx) and receiving antenna (Rx) are set at fixed places, where the distances between the prototype and two antennas are d^i and d^r, respectively. During the measurement, the distances of d^i and d^r are both selected as 1.5m to meet the far-field condition [35]. To further minimize the error in measurement, the calibration method in [36] is applied. By changing the positions of two antennas, this measurement system can work for different incident angles.

Fig. 8 illustrates the synthetizations, simulations, and measurements of the proposed 3-D absorber-I under normal incidence. The synthesized results are obtained based on the equivalent TL model using the synthesis approach in Section II. For the simulation, periodic boundary conditions and floquet ports are employed to obtain an infinite

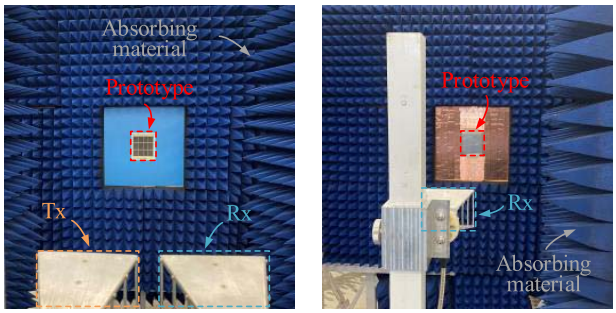

FIGURE 7. Photographs of testing set-up. (a) Reflection coefficient measurement. (b) Transmission coefficient measurement.

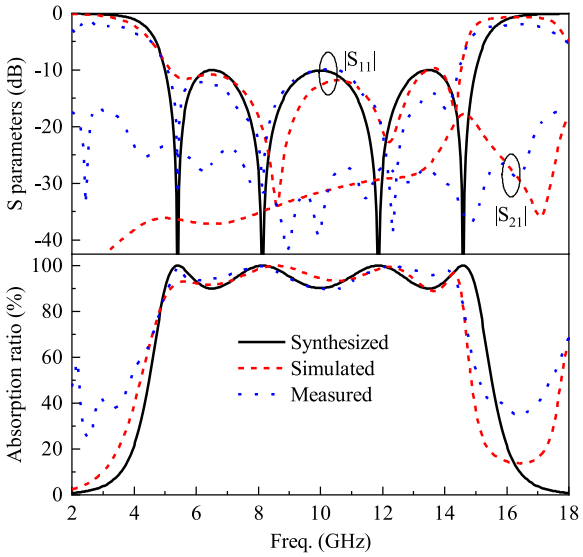

FIGURE 8. Synthesized, simulated and measured results of the proposed 3-D absorber-I under normal incidence.

array structure. Different from the ideal equivalent model, not all the spatial wave can be perfectly converted into guided waves. Here, the input spatial wave is provided by the upper floquet port (port 1) while the underside floquet port (port 2) is utilized to detect the undesired leaked spatial wave. The measured results are from the finite-sized prototype. As observed, synthetizations, simulations, and measurements are in good agreement within the operating band. The differences between measurements and simulations are mainly due to: 1) the larger loss of the actual substrate, and 2) unavoidable errors during the measurement, such as the introduction of the fixer, the accuracy of the manual testing system, and the deviation of calibration processing.

The simulated and measured FBWs are 94.9% (from 5.18 to 14.54GHz) and 95.5% (from 5.08 to 14.44GHz), respectively. Within the operating band, the S_{21} for simulation and measurement are less than -17.8dB and -23.5dB. The simulated and measured average in-band absorption ratios are higher than 95.0% and 95.5%. Here, the absorption ratio is

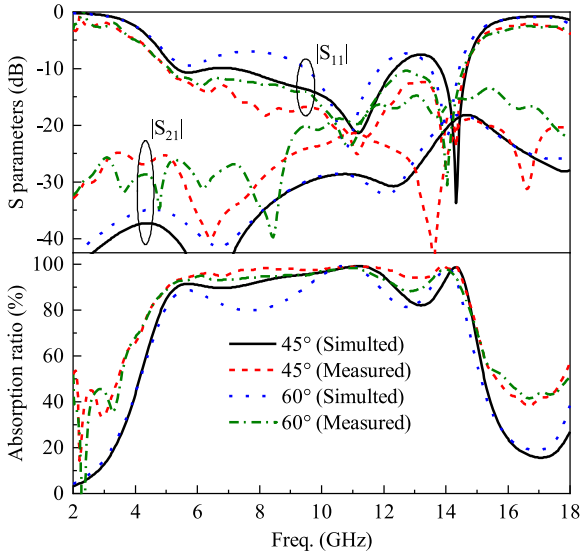

FIGURE 9. Simulated and measured results of the proposed 3-D absorber-I under oblique incidence at YOZ plane.

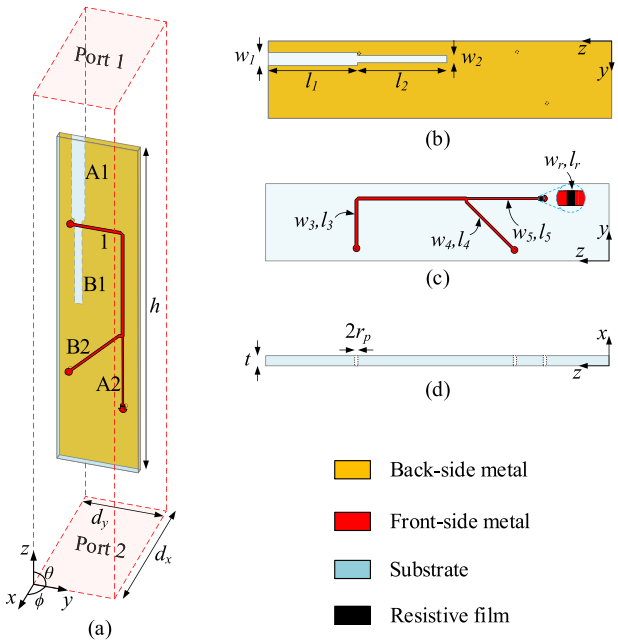

FIGURE 10. Element geometry of the proposed 3-D absorber-II. (a) Perspective view. (b) Back view. (c) Front view. (d) Side view.

calculated by

$$\text{Absorption ratio} = \sqrt{1 - |S_{11}|^2 - |S_{21}|^2} \tag{3}$$

The simulated and measured results of the proposed 3-D absorber-I under oblique incidence at YOZ plane are further comparatively investigated and described in Fig. 9. It can be seen that measured results agree well with simulations. Under the condition of 45° oblique incidence, the simulated and measured 80% absorption ratio bandwidths are 101.4% (from 4.84 to 14.8GHz) and 107.1% (from 4.48 to 14.8GHz).

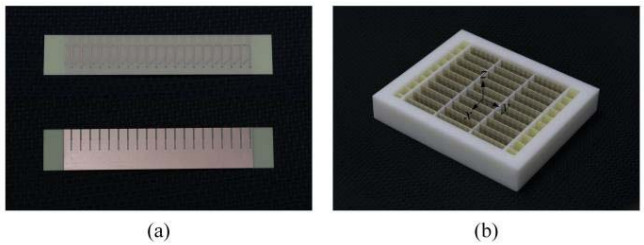

FIGURE 11. Photographs of the proposed 3-D absorber-II. (a) Substrate pieces. (b) Final prototype.

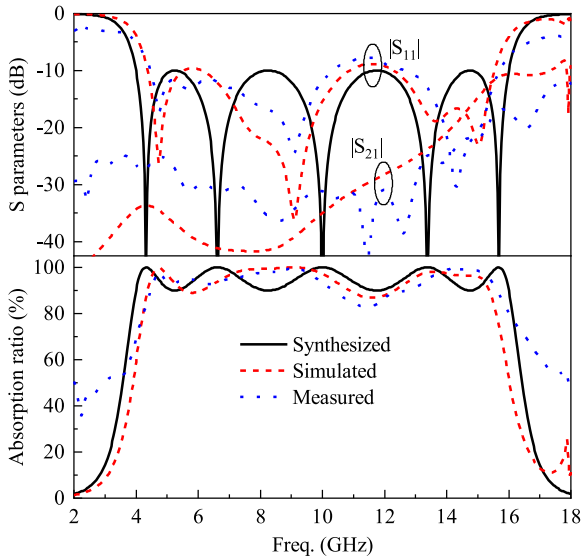

FIGURE 12. Synthesized, simulated and measured results of the proposed 3-D absorber-II under normal incidence.

TABLE 2. Geometrical parameters of the proposed 3-D absorber-II.

Parameter	d_x	d_y	h	t	w_1	l_1
Value (mm)	9	4.5	20	0.5	0.75	5.2
Parameter	w_2	l_2	w_3	l_3	w_4	l_4
Value (mm)	0.43	5.2	0.18	9.3	0.14	4.2
Parameter	w_5	l_5	w_r	l_r	r_p	
Value (mm)	0.12	4.2	0.22	0.11	0.1	

TABLE 3. Comparisons of the proposed 3-D absorber-I ($i = 1$).

	Synthesis	Simulation	Measurement
-10dB lower cutoff frequency	5GHz	5.18GHz	5.08GHz
Maximum in-band transmission coefficient	-	-17.8dB	-23.5dB
Average in-band absorption ratio	94.9%	95.0%	95.5%
-10dB upper cutoff frequency	15GHz	14.54GHz	14.44GHz

TABLE 4. Comparisons of the proposed 3-D absorber-II ($i = 2$).

	Synthesis	Simulation	Measurement
-10dB lower cutoff frequency	4GHz	4.37GHz	4.48GHz
Maximum in-band transmission coefficient	-	-11.6dB	-16.9dB
Average in-band absorption ratio	94.9%	94.8%	93.8%
-10dB upper cutoff frequency	16GHz	15.54GHz	15.68GHz

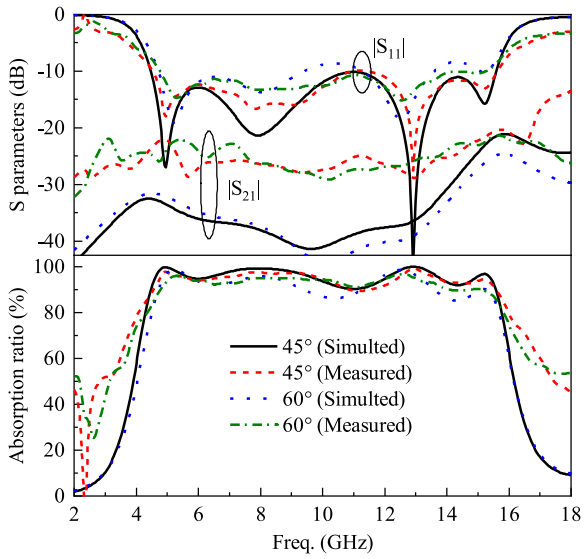

FIGURE 13. Simulated and measured results of the proposed 3-D absorber-II under oblique incidence at YOZ plane.

For 60° oblique incidence, the 80% absorption ratio bandwidths of 98.7% (from 4.96 to 14.6GHz) and 106.2% (from 4.52 to 14.76GHz) are still well obtained for simulations and measurements. These results clearly exhibit that using the structure of composite slotlines and microstrip lines, the proposed absorber-I indeed realizes an ultra-wideband absorptive performance under a large variety of incident angles.

B. ABSORBER-II

Fig. 10 shows the element configuration of the proposed 3-D absorber-II ($i = 2$), which is similar to that of absorber-I. With the desired absorptive performances of $\Gamma = -10$dB, FBW $= 120\%$, the normalized characteristic impedances are calculated as $z_a = 0.52$, $z_b = 0.51$, and $z_1 = 0.43$. Here, the input impedance is set as $Z_0 = 188$Ohm. Table 2 tabulates the detailed geometrical parameters.

The detailed photographs of the proposed 3-D absorber-II are shown in Fig. 11. As can be seen in Fig. 11(a), each set of 20 elements is printed on a long piece of substrate. The total size of the substrate for absorber-II is 110mm×20mm. In Fig. 11(b), by inserting the substrate into securing slots, the fabricated prototype with 10×20 elements is completed.

Fig. 12 shows the synthetizations, simulations, and measurements of the proposed 3-D absorber-II under normal incidence. As seen, measurements agree well again with synthetizations and simulations. The simulated and measured

TABLE 5. Comparisons between the proposed design and other reported 3-D absorbers.

Ref.	Absorption bandwidth	Angular stability	Design method	No. of substrate	No. of resistive load	Thickness (λ_L)
[19]	63.8% (4.8GHz~9.3GHz)	40° (90%) (Only simulated)	Equivalent circuit model	3	1	0.31
[24]	156.6% (1.5GHz~12.31GHz)	45° (Only simulated)	Equivalent circuit model	6	4	0.1
[29]	85.8% (6.95GHz~17.4GHz)	65° (AR>80%)	Optimize the SSPP structure	4	18	0.18
[30]	59.3% (2.11GHz~3.89GHz)	60° (AR>80%) (Only simulated)	Multiple resistive resonances control	5	8	0.09
Prop. Absorber-I	**95.5% (5.08GHz~14.44GHz)**	**60° (AR>80%)**	**Synthetic design based on Equivalent TL model**	**1**	**1**	**0.22**
Prop. Absorber-II	**111.1% (4.48GHz~15.68GHz)**	**60° (AR>80%)**	**Synthetic design based on Equivalent TL model**	**1**	**1**	**0.29**

λ_L is the wavelength at the lowest frequency in free space.

FBWs are 112.2% (from 4.37 to 15.54GHz) and 111.1% (from 4.48 to 15.68GHz), respectively. The simulated and measured S_{21} magnitudes within the operating band are less than −11.6dB and −16.9dB. The simulations and measurements of average in-band absorption ratios are higher than 94.8% and 93.8%.

Fig. 13 describes the simulated and measured results of the proposed 3-D absorber-II under oblique incidence at YOZ plane. Good agreement can be observed between measured and simulated results. For the 45° oblique incidence, the 80% absorption ratio bandwidths of 113.9% (from 4.32 to 15.76GHz) and 117.9% (from 4.12 to 15.96GHz) are realized for simulations and measurements. In the case of 60° oblique incidence, the simulated and measured 80% absorption ratio bandwidths are 110.3% (from 4.52 to 15.64GHz) and 112.9% (from 4.4 to 15.8GHz). These results indicate that the ultra-wideband absorptive performance can be successfully obtained by the proposed absorber-II under not only normal incidence, but also oblique incidence.

As a brief summary, two prototypes of absorber-I and absorber-II have been theoretically designed and practically implemented. Table 3 and Table 4 illustrate the comparisons for these two absorbers, showing that the input spatial wave can be effectively absorbed by using the proposed structures. The realized absorptive performances are very close to the expectation, which obviously proves the proposed design concept. Table 5 shows the comparisons between our designs and other reported 3-D absorbers. It can be figured out that the proposed 3-D absorbers can be quickly designed using the presented equivalent TL model and synthesis approach, which leads to the ultra-wideband absorptive performance with a single-layered substrate and only one resistive load along a single absorber element. It should be noted that the proposed absorbers in this work are not placed above a metal plate. Considering the practical scenario where a metal object is presented behind the absorber, the proposed design can keep absorptive performances almost unchanged. This applicability can be attributed to the effectiveness of conversion from spatial waves to guided waves and absorption from the loaded resistor.

IV. CONCLUSION

In this article, the class of ultra-wideband 3-D microwave absorbers has been presented with synthetic design and practical implementation. Based on the equivalent transmission line model, the synthetic procedure of the proposed absorber element is theoretically investigated and executed, so as to explicitly establish the relationship between specific absorptive performance and network parameters. To validate the proposed concept, two prototypes with a simple 3-D structure composed of composite slotlines and microstrip lines are designed, fabricated, and tested. Measurements agree

$$\begin{cases} k_1 = \frac{-(z_a+1)(z_a-1)[(z_b+z_1)z_a+z_bz_1]}{2{z_a}^2{z_b}^2z_1} \\ k_2 = \frac{\left[-\left(-{z_1}^2-2z_bz_1-2{z_b}^2\right){z_a}^4+2{z_a}^3z_bz_1(z_b+z_1)+{z_a}^2{z_b}^2\left({z_1}^2-1\right)-2z_az_bz_1(z_b+z_1)-2{z_b}^2{z_1}^2\right]}{2{z_a}^2{z_b}^2z_1} \\ k_3 = \frac{-{z_a}^4{z_b}^2+{z_b}^2{z_1}^2}{2{z_a}^2{z_b}^2z_1} \end{cases} \tag{A-1}$$

$$\begin{cases} l_1 = \frac{-(z_a+1)(z_a-1)[(z_b+z_1)z_a+z_bz_1]^2}{{z_a}^2{z_b}^2z_1} \\ l_2 = \frac{\left[(2z_b+z_1){z_a}^3+{z_a}^2z_bz_1-z_az_b-2z_bz_1\right][(z_b+z_1)z_a+z_bz_1]}{{z_a}^2{z_b}^2z_1} \\ l_3 = \frac{z_b\left[(-z_b-z_1){z_a}^4-{z_a}^3z_bz_1+z_az_bz_1+z_b{z_1}^2\right]}{{z_a}^2{z_b}^2z_1} \end{cases} \tag{A-2}$$

well with synthesized and simulated results, showing the ultra-wideband absorptive performance under a large variety of incident angles. Therefore, it is our belief that such 3-D microwave absorbers possess the attractive potential for EM waves absorption.

APPENDIX

The coefficients of k_1–k_3 and l_1–l_3 are given in (A-1) and (A-2), respectively, at the bottom of the previous page.

ACKNOWLEDGMENT

The authors would like to sincerely thank Yun-Jie Zhu, and Prof. Bo Li with Nanjing University of Posts and Telecommunications for their kind assistance during the prototype measurement. They would also like to thank Ohmega for providing the resistive film and Wake Material Technology (Shenzhen) for the technical support.

REFERENCES

[1] W. Emerson, "Electromagnetic wave absorbers and anechoic chambers through the years," *IEEE Trans. Antennas Propag.*, vol. AP-21, no. 4, pp. 484–490, Jul. 1973.

[2] K. J. Vinoy and R. M. Jha, *Radar Absorbing Materials: From Theory to Design and Characterization*. Norwood, MA, USA: Kluwer Acad., 1996.

[3] W. W. Salisbury, "Absorbent body for electromagnetic waves," U.S. Patent 2 599 944, Jun. 1952.

[4] L. J. D. Toit and J. H. Cloete, "Electric screen Jauman absorber design algorithms," *IEEE Trans. Microw. Theory Techn.*, vol. 44, no. 12, pp. 2238–2245, Dec. 1996.

[5] Y. Naito and K. Suetake, "Application of ferrite to electromagnetic wave absorber and its characteristics," *IEEE Trans. Microw. Theory Techn.*, vol. MTT-19, no. 1, pp. 65–72, Jan. 1971.

[6] H. Choo, H. Ling, and C. S. Liang, "On a class of planar absorbers with periodic square resistive patches," *IEEE Trans. Antennas Propag.*, vol. 56, no. 7, pp. 2127–2130, Jul. 2008.

[7] B. Xu, C. Gu, Z. Li, L. Liu, and Z. Niu, "A novel absorber with tunable bandwidth based on graphene," *IEEE Antennas Wireless Propag. Lett.*, vol. 13, pp. 822–825, 2014.

[8] T. Deng, Z.-W. Li, and Z. N. Chen, "Ultrathin broadband absorber using frequency-selective surface and frequency-dispersive magnetic materials," *IEEE Trans. Antennas Propag.*, vol. 65, no. 11, pp. 5886–5894, Nov. 2017.

[9] Y. Tayde, M. Saikia, K. V. Srivastava, and S. A. Ramakrishna, "Polarization-insensitive broadband multilayered absorber using screen printed patterns of resistive ink," *IEEE Antennas Wireless Propag. Lett.*, vol. 17, pp. 2489–2493, 2018.

[10] X. Zhang et al., "3-D printed swastika-shaped ultrabroadband water-based microwave absorber," *IEEE Antennas Wireless Propag. Lett.*, vol. 19, pp. 821–825, 2020.

[11] W. Li, X. Chen, Z. Zhang, Z. Wu, L. Yang, and Y. Zou, "Ultralight and low-cost structural absorbers with enhanced microwave absorption performance based on sustainable waste biomass," *IEEE Trans. Antennas Propag.*, vol. 70, no. 1, pp. 401–409, Jan. 2022.

[12] J. Wen, Q. Ren, R. Peng, and Q. Zhao, "Ultrabroadband saline-based metamaterial absorber with near theoretical absorption bandwidth limit," *IEEE Antennas Wireless Propag. Lett.*, vol. 21, pp. 1388–1392, 2022.

[13] Y. Shang, Z. Shen, and S. Xiao, "On the design of single-layer circuit analog absorber using double-square-loop array," *IEEE Trans. Antennas Propag.*, vol. 61, no. 12, pp. 6022–6029, Dec. 2013.

[14] Y. Han, W. Che, X. Xiu, W. Yang, and C. Christopoulos, "Switchable low-profile broadband frequency-selective rasorber/absorber based on slot arrays," *IEEE Trans. Antennas Propag.*, vol. 65, no. 12, pp. 6998–7008, Dec. 2017.

[15] B. Zhang, C. Jin, and Z. Shen, "Low-profile broadband absorber based on multimode resistor-embedded metallic strips," *IEEE Trans. Microw. Theory Techn.*, vol. 68, no. 3, pp. 835–843, Mar. 2020.

[16] J. Mou and Z. Shen, "Design and experimental demonstration of non-Foster active absorber," *IEEE Trans. Antennas Propag.*, vol. 65, no. 2, pp. 696–704, Feb. 2017.

[17] Y. Zhang, Z. Cao, Z. Huang, L. Miao, S. Bie, and J. Jiang, "Ultrabroadband double-sided and dual-tuned active absorber for UHF band," *IEEE Trans. Antennas Propag.*, vol. 69, no. 2, pp. 1204–1208, Feb. 2021.

[18] A. K. Rashid, Z. Shen, and S. Aditya, "Wideband microwave absorber based on a two-dimensional periodic array of microstrip lines," *IEEE Trans. Antennas Propag.*, vol. 58, no. 12, pp. 3913–3922, Dec. 2010.

[19] B. Li and Z. Shen, "Wideband 3D frequency selective rasorber," *IEEE Trans. Antennas Propag.*, vol. 62, no. 12, pp. 6536–6541, Dec. 2014.

[20] Z. Shen, J. Wang, and B. Li, "3-D frequency selective rasorber: Concept, analysis, and design," *IEEE Trans. Microw. Theory Techn.*, vol. 64, no. 10, pp. 3087–3096, Oct. 2016.

[21] A. A. Omar and Z. Shen, "Double-sided parallel-strip line resonator for dual-polarized 3-D frequency-selective structure and absorber," *IEEE Trans. Microw. Theory Techn.*, vol. 65, no. 10, pp. 3744–3752, Oct. 2017.

[22] H. Huang, Z. Shen, and A. A. Omar, "3-D absorptive frequency selective reflector for antenna radar cross section reduction," *IEEE Trans. Antennas Propag.*, vol. 65, no. 11, pp. 5908–5917, Nov. 2017.

[23] A. A. Omar, Z. Shen, and H. Huang, "Absorptive frequency-selective reflection and transmission structures," *IEEE Trans. Antennas Propag.*, vol. 65, no. 11, pp. 6173–6178, Nov. 2017.

[24] G. Q. Luo, W. Yu, Y. Yu, X. H. Zhang, and Z. Shen, "A three-dimensional design of ultra-wideband microwave absorbers," *IEEE Trans. Microw. Theory Techn.*, vol. 68, no. 10, pp. 4206–4215, Oct. 2020.

[25] S. Ghosh and S. Lim, "Perforated lightweight broadband metamaterial absorber based on 3-D printed honeycomb," *IEEE Antennas Wireless Propag. Lett.*, vol. 17, pp. 2379–2383, 2018.

[26] F. He et al., "Frequency selective surface composites with honeycomb absorbing structure for broadband applications," *IEEE Trans. Antennas Propag.*, vol. 70, no. 9, pp. 8643–8647, Sep. 2022.

[27] T. Deng, Y. Yu, Z. Shen, and Z. N. Chen, "Design of 3-D multilayer ferrite-loaded frequency-selective rasorbers with wide absorption bands," *IEEE Trans. Microw. Theory Techn.*, vol. 67, no. 1, pp. 108–117, Jan. 2019.

[28] Y. Wang, S.-S. Qi, Z. Shen, and W. Wu, "Ultrathin 3-D frequency selective rasorber with wide absorption bands," *IEEE Trans. Antennas Propag.*, vol. 68, no. 6, pp. 4697–4705, Jun. 2020.

[29] J. Yu, W. Jiang, and S. Gong, "Wideband angular stable absorber based on spoof surface plasmon polariton for RCS reduction," *IEEE Antennas Wireless Propag. Lett.*, vol. 19, pp. 1058–1062, 2020.

[30] T. Shi, L. Jin, L. Han, M.-C. Tang, H.-X. Xu, and C.-W. Qiu, "Dispersion-engineered, broadband, wide-angle, polarization- independent microwave metamaterial absorber," *IEEE Trans. Antennas Propag.*, vol. 69, no. 1, pp. 229–238, Jan. 2021.

[31] Y.-T. Zhao, B. Chen, and B. Wu, "Miniaturized periodicity broadband absorber with via-based hybrid metal-graphene structure for large-angle RCS reduction," *IEEE Trans. Antennas Propag.*, vol. 70, no. 4, pp. 2832–2840, Apr. 2022.

[32] H. Huang, C. Hua, and Z. Shen, "Absorptive frequency-selective transmission structures based on hybrid FSS and absorber," *IEEE Trans. Antennas Propag.*, vol. 70, no. 7, pp. 5606–5613, Jul. 2022.

[33] L. Zhu, S. Sun, and R. Li, *Microwave Bandpass Filters for Wideband Communications*. Hoboken, NJ, USA: Wiley, 2012.

[34] R. Li, S. Sun, and L. Zhu, "Synthesis design of ultra-wideband bandpass filters with composite series and shunt stubs," *IEEE Trans. Microw. Theory Techn.*, vol. 57, no. 3, pp. 684–692, Mar. 2009.

[35] C. A. Balanis, *Antenna Theory Analysis and Design*, 3rd ed. New York, NY, USA: Wiley, 2005.

[36] M. Al-Joumayly and N. Behdad, "A new technique for design of low-profile, second-order, bandpass frequency selective surfaces," *IEEE Trans. Antennas Propag.*, vol. 57, no. 2, pp. 452–459, Feb. 2009.

TIAN-XI FENG (Graduate Student Member, IEEE) was born in Yichun, Heilongjiang, China, in 1994. He received the B.S. and M.Eng. degrees from Xidian University, Xi'an, China, in 2017 and 2020, respectively. He is currently pursuing the Ph.D. degree in electrical and computer engineering with the University of Macau, Macau, China.

His research interests include pattern manipulation structures, antenna arrays, and 3-D microwave absorbers.

LEI ZHU (Fellow, IEEE) received the B.Eng. and M.Eng. degrees in radio engineering from the Nanjing Institute of Technology (currently, Southeast University), Nanjing, China, in 1985 and 1988, respectively, and the Ph.D. degree in electronic engineering from the University of Electro-Communications, Tokyo, Japan, in 1993.

From 1993 to 1996, he was a Research Engineer with Matsushita-Kotobuki Electronics Industries Ltd., Tokyo. From 1996 to 2000, he was a Research Fellow with the École Polytechnique de Montréal, Montreal, QC, Canada. From 2000 to 2013, he was an Associate Professor with the School of Electrical and Electronic Engineering, Nanyang Technological University, Singapore. He joined the Faculty of Science and Technology, University of Macau, Macau, China, as a Full Professor in August 2013, where he has been a Distinguished Professor since December 2016. From August 2014 to August 2017, he served as the Head of the Department of Electrical and Computer Engineering, University of Macau. So far, he has authored or coauthored more than 750 papers in international journals and conference proceedings. His papers have been cited more than 15 000 times with the H-index of 61 (source: Scopus). His research interests include microwave circuits, antennas, periodic structures, and computational electromagnetics.

Dr. Zhu was the recipient of the 1997 Asia–Pacific Microwave Prize Award, the 1996 Silver Award of Excellent Invention from Matsushita-Kotobuki Electronics Industries Ltd., the 1993 Achievement Award in Science and Technology (First Prize) from the National Education Committee of China, the 2020 FST Research Excellence Award from the University of Macau, and the 2020 and 2022 Macao Natural Science Awards (Second Prize) from the Science and Technology Development Fund (FDCT), Macau. He was an Associate Editor of the IEEE TRANSACTIONS ON MICROWAVE THEORY AND TECHNIQUES from 2010 to 2013 and IEEE MICROWAVE AND WIRELESS COMPONENTS LETTERS from 2006 to 2012. He served as the General Chair of the 2008 IEEE MTT-S International Microwave Workshop Series on the Art of Miniaturizing RF and Microwave Passive Components, Chengdu, China, and a Technical Program Committee Co-Chair of the 2009 Asia–Pacific Microwave Conference, Singapore. He served as a member of the IEEE MTT-S Fellow Evaluation Committee from 2013 to 2015 and the IEEE AP-S Fellows Committee from 2015 to 2017.